Int. J. Environ. Sci. Technol. (2016) 13:973–984
DOI 10.1007/s13762-015-0929-4

ORIGINAL PAPER

Removal of sulfamethazine antibiotics using cow manure-based carbon adsorbents

T.-W. Tzeng[1] · Y.-T. Liu[1] · Y Deng[2] · Y.-C. Hsieh[3] · C.-C. Tan[1] · S.-L. Wang[4] · S.-T. Huang[1,5] · Y.-M. Tzou[1]

Received: 28 July 2015 / Revised: 3 December 2015 / Accepted: 14 December 2015 / Published online: 7 January 2016

Abstract Low-cost adsorbents, e.g., cow manure-based carbon, provide alternatives to remove veterinary antibiotic sulfamethazine (SMT) from contaminated water bodies. In this study, the chemical structures and compositions of cow manure (CM) carbonized at 400, 600, and 800 °C (CM400, CM600, and CM800) were examined using elemental analyzer (EA), Brunauer–Emmett–Teller, and spectroscopic techniques. Adsorptions of SMT on CM samples were conducted as functions of pH, hydrophobicity, and ionic strengths. Results of EA and spectroscopic analyses suggested that the raw CM and CM400 samples contained the highest amounts of O-containing groups and aliphatic domains. Amounts of such two chemical groups decreased as carbonization temperatures increased. The specific surface areas and total pore volumes of CM samples increased significantly when the carbonization temperatures exceeded 600 °C. SMT adsorption on CM samples could be described essentially by the pseudo-second-order kinetic, intra-particle diffusion, and Freundlich isotherm models. Low pH and ionic strength were favorable for SMT adsorption in CM samples, particularly for the CM800, because a strong π^{+}–π electron donor–acceptor interaction (π^{+}–π EDA) was formed between SMT and CM surfaces enriched with hydrophobic domains. Further, the high adsorption affinity of SMT to the CM600 and CM800 samples was attributed in part to their larger surface areas and total pore volumes. Generally, CM-based materials carbonized >600 °C showed relatively stable structures and exhibited strong aromatic properties. Moreover, maximum adsorption capacities of SMT on the CM800 sample (37–39 mM/kg) were significantly higher than those of other common adsorbents (0.02–35.93 mM/kg).

Keywords Sulfonamide · Animal wastes · Carbonization · Adsorption · π^{+}–π EDA

Electronic supplementary material The online version of this article (doi:10.1007/s13762-015-0929-4) contains supplementary material, which is available to authorized users.

✉ Y.-M. Tzou
ymtzou@dragon.nchu.edu.tw

[1] Department of Soil and Environmental Sciences, National Chung Hsing University, 250 Kuo-Kuang Rd. (or 145 Xingda Rd.), Taichung 40227, Taiwan, ROC

[2] Department of Soil and Crop Sciences, Texas A&M University, College Station, TX 77843, USA

[3] Office of the Texas State Chemist, Texas A&M AgriLife Research, Texas A&M University System, College Station, TX 77843, USA

[4] Department of Agricultural Chemistry, National Taiwan University, Taipei, Taiwan, ROC

[5] Department of Science Education and Application, National Taichung University of Education, Taichung, Taiwan, ROC

Introduction

Pharmaceutical antibiotics (PAs) are used widely in the livestock and poultry industries to improve the efficiency of feed use, promote growth rate, and reduce mortality and morbidity (Barbooti et al. 2014). Because these PAs can bio-accumulate, they pose a long-term risk to aquatic and terrestrial organisms upon their release into the environment, even if the concentrations of PAs in nature are relatively low (range of μg/L to ng/L) (Bui et al. 2013; Kümmerer 2009). Besides, sulfonamides may constitute a serious threat to public health and ecosystems due to the potential spread of antibiotic resistance within bacterial communities (Hou et al. 2014).

Sulfonamides (SAs), derived primarily from sulfanilamide, are organic sulfur compounds with a functional group of $–SO_2NH_2–$. They are among the pharmaceutical antibiotics used to treat or prevent bacterial infection, diabetes mellitus, edema, hypertension, and gout-associated problems (Hiba et al. 2016). In European countries, sulfonamides are one of the groups of antibiotics administered most widely in animal husbandry; approximately 363,000 kg of sulfamethazine (SMT), a group of sulfonamides, is used in swine production every year (Li et al. 2013; Raich-Montiu et al. 2007). Unfortunately, sulfonamides are only metabolized partially in animals after therapeutic treatments, and it has been estimated that approximately 30–90 % of antibiotics are excreted through urine and feces (Zessel et al. 2014). Due to ineffective or inappropriate treatment of these animal wastes, the antibiotics are discharged ultimately into the environments (Bao et al. 2014; Schwab et al. 2005; Tamtam et al. 2008). As a result, the sulfonamides are found frequently in the surface/ground water, soils, sediments, and even in the drinking water (Batt et al. 2006; Heberer 2002).

Richter et al. (2007) investigated the concentrations of para-toluenesulfonamide (*p*-TSA) in different bodies of water systemically, and a maximum *p*-TSA concentration of 50.8 μg/L was observed in the aquatic media. Lin et al. (2013) reported that 0.05 mg/L sulfamethoxazole (SMZ) was detected in the surface waters and sewage treatment plant effluents in the UK. In addition, sulfonamides have been found commonly in soil systems that received the antibiotic-containing wastes. For example, Christian et al. (2003) indicated that approximately 0.015 mg/kg of sulfonamides accumulated in different soils fertilized with animal manure. García-Galán et al. (2013) traced the concentrations of 22 sulfonamide antibiotics and their metabolites in the sewage sludge and soil samples and reported that a maximum concentration of 8.53 ng/g of sulfonamides was found in these media.

Sulfonamides interact with soils through a complex process that is affected by various factors, such as pH, ionic strength, exchangeable cations, and the composition of soil organic matter (Leal et al. 2013; Srinivasan et al. 2014). Kurwadkar et al. (2007) found a significant increase in the adsorption of sulfonamides in three loamy soils when the sulfonamides were converted from anionic forms with higher pH to neutral/cationic forms with a lower pH. Srinivasan et al. (2014) reported that the adsorption of three sulfonamide compounds: sulfamethoxazole (SMO), sulfachloropyridazine (SCP), and SMT, in six top soils was controlled by both cation exchange capacity (CEC) and organic carbon content. Even if soils exhibited some ability to adsorb sulfonamides, the force of adsorption seemed unlikely to inhibit plant uptake completely. For instance, Li et al. (2013) found a relatively high concentration of SMT and sulfamethoxazole (SMZ) in pakchoi cabbage compared with sulfadiazine (SDZ), because the plant was grown in soils with a higher residual concentration of SMT and SMZ. These results suggested that a portion of sulfonamides/antibiotics was bioavailable to plants, even if sulfonamides could be adsorbed by soils.

To avoid/prevent the detrimental effects of sulfonamides on ecosystems, the development of advanced oxidation processes or preparations of efficient adsorbents is still necessary to scavenge the antibiotics found in the environment. Several advanced oxidation techniques, such as electro-Fenton (Mansour et al. 2015), photoelectrocatalysis (Hu et al. 2007; Kaniou et al. 2005), sonolysis (Gao et al. 2013), and the photo-Fenton process (Perez-Moya et al. 2010), had been used successfully to remove the antibiotics or their metabolites. However, high costs and the presence of high organic compounds in the antibiotics-bearing media may hinder their practical applications.

Adsorption is an alternative approach to remove antibiotics due to its low cost and easy application. Various adsorbents, including carbon nanotubes (Ji et al. 2009), zeolite (Braschi et al. 2010), activated carbon (Valderrama et al. 2007), and chitosan (Vieira et al. 2007), had been used to remove SMT antibiotics. Although these adsorbents show promising efficiency in sulfonamide antibiotics removal, the search for new adsorbents, particularly those derived from agricultural wastes, is still needed. In Taiwan, two hundred thousand cows produce 1.5 hundred million tons of animal wastes annually. The primary form of treatment for this excrement is composting, including vermicomposting, a process that requires several weeks to months to convert animal feces to useful fertilizers (Lim et al. 2015a). However, antibiotics or pharmaceuticals in the manures may not be decomposed completely during the composting process, which can lead to the potential transfer of antibiotics into, or bacterial resistance of soils to which manure-containing fertilizers are applied (Kim et al. 2012; Lillenberg et al. 2010). Moreover, antibiotics may inhibit the growth of earthworms during the vermicomposting process (Lim et al. 2015b). Thus, composting may not be an appropriate choice in treating animal wastes that contain antibiotics.

Pyrolysis is a rapid and incomplete combustion process that converts biomaterials into biochar (Liu et al. 2012; Wang and Xing 2007). Because sulfonamide antibiotics are unstable at high temperatures, pyrolysis may be an alternative method to convert cow manure to a useful bio-adsorbent that is free of residual antibiotics. The structure of biochar is similar to that of activated carbon and consists primarily of short stacks of graphite sheets with O-containing groups on the edge (Ji et al. 2011). Biochar shows a strong adsorption affinity for hydrophobic organic contaminants due to its large specific surface areas (SSAs) and

high surface hydrophobicity (Xie et al. 2014). Our goal in this study was to determine the efficiency of SMT removal by cow manure-based carbon that was carbonized at three temperatures (400, 600, and 800 °C), denoted as CM400, CM600, and CM800, respectively. The surface functional groups and chemical compositions of the CM samples with and without temperature treatments were examined first by BET, element analysis, and spectroscopic techniques. The effects of pH and ionic strength on SMT adsorption in CM were evaluated by kinetic and isotherm models to address the dominant driving force of SMT adsorption on CMs. With the exception of the BET and NMR analyses, each experiment was carried out in 2013 in the Department of Soil and Environmental Sciences of National Chung Hsing University, Taiwan.

Materials and methods

Preparation of carbon black from cow manure

Raw cow manure (RCM), collected from the Livestock Research Institute in Taiwan, was carbonized at 400, 600, and 800 °C in a furnace sparged continuously with nitrogen gas at a flow rate of 100 mL/min. Hereafter, the carbonized samples are denoted as CM400, CM600, and CM800. The carbon black samples were then washed with 3 M hydrochloride (HCl) followed by de-ionized water to remove silicate and soluble salts. After freeze-drying for 24 h, carbon black samples were ground slightly, passed through a 60-mesh sieve, and stored in a plastic bottle for further use.

Characterizations of carbon black

The surface functional groups of the adsorbents, including RCM and its derivative carbon black samples, were determined using Fourier transform infrared spectroscopy (FTIR, thermo Nicolet NexusTM Microscope Spectrometer) with a DRIFT accessory (Spectros Instruments). Each spectrum was recorded with a mixture of 10 mg CM and 390 mg of KBr under nitrogen purge. Solid-state ^{13}C cross-polarization/magic angle spinning (CP/MAS) NMR spectra with a 4 mm DR MAS probe (JCAMP, Bruker, USA) was used to analyze the chemical structures, and an Element Analyzer (Heraeus varioIII-NCH, Germany) was used to determine the C, H, and O compositions of the CM samples. The SSA and porosity were obtained according to the Brunauer–Emmett–Teller (BET) method, on the basis of the measurements relating to N_2 adsorption with an apparatus at 77 K (Micromeritics ASAP 2020, USA). The morphology of each CM sample was observed with a field emission scanning electron microscope (JSM-7401F; JEOL, Japan). The pH zero point charge (pH_{zpc}) of each CM sample was obtained by a pH drift method (Lopez-Ramon et al. 1999; Putra et al. 2009; Shirzad-Siboni et al. 2015).

Adsorption experiments

The adsorption kinetics and adsorption isotherm of SMT (purchased from Sigma-Aldrich with a purity of 99 % and used as received) onto CM400, CM600, and CM800 were carried out in a batch mode. A SMT stock solution of 100 mg/L was prepared freshly and stored in the dark at 4 °C prior to the experiments. The suspension concentration of the CM-derived carbon black sample was controlled at 2 g/L. A circulating water bath was used to maintain the reaction temperature at 25 ± 1 °C. 0.10 M HCl and KOH solutions were used to adjust the suspension pH. Ten ml suspensions were sampled periodically and filtered through a 0.20 μm pore size, cellulose acetate membrane filter. The SMT in the filtrate was determined colorimetrically at 262 nm using a Spectro UV-2550 UV–visible spectrophotometer (Labomed, USA). Preliminary studies suggested that the effects of pH (3–11) on SMT absorbance at 262 nm were slight, but the dissoluble organic carbon (DOC) derived from the CM samples, particularly for CM400, interfered significantly with the measurement of SMT. To obtain its precise concentrations, the increase in the absorbance at 262 nm due to the presence of DOC was deducted for each pH tested, while using the linear region of the SMT calibration curve to calculate the concentration. In addition, 2 mL of NaH_2BO_3 buffer solutions (pH 10) was added to 8 mL of filtrate before determining the SMT concentrations to avoid pH-dependent changes in SMT species during HPLC analyses (Ji et al. 2009; Wang et al. 2014; Xie et al. 2014).

Adsorption isotherm of SMT was performed by adding initial SMT concentrations of 5, 10, 20, 30, 50, 70, and 100 mg/L into a 0.04 g CM sample (1 g/L), followed by 12 h of reaction. The effects of ionic strengths (i.e., 5 and 500 mM KCl) and pH (3, 8, and 10) on SMT adsorption were also evaluated in the reactions vessels at a constant temperature of 25 ± 1 °C.

Speciation modeling

Depending on the pH of the solution, SMT can exist as a cation (SMT^+), anion (SMT^-), uncharged molecule (SMT^0), or zwitterion ($SMT^\pm$) upon H^+ dissociation or protonation at the aromatic amine and sulfonamide groups ($pK_{a1} = 2.6$ $pK_{a2} = 7.4$) (Pinna et al. 2012; Tolls 2001) (Fig. S1). The mass fractions of such sulfamethazine species (Fig. S2) can be quantified as a function of pH and pK_a

values, as described in Eqs. (1)–(3) (Kurwadkar et al. 2007).

$$\alpha_0 = \frac{1}{1 + 10^{(\mathrm{pH}-\mathrm{p}K_1)} + 10^{(2\mathrm{pH}-\mathrm{p}K_1-\mathrm{p}K_2)}} \quad (1)$$

$$\alpha_1 = \frac{1}{1 + 10^{(\mathrm{p}K_1-\mathrm{pH})} + 10^{(\mathrm{pH}-\mathrm{p}K_2)}} \quad (2)$$

$$\alpha_2 = \frac{1}{1 + 10^{(\mathrm{p}K_2-\mathrm{pH})} + 10^{(\mathrm{p}K_1+\mathrm{p}K_2-2\mathrm{pH})}} \quad (3)$$

where pK_1 and pK_2 are the first and second dissociation constants of SMT, respectively, and α_0, α_1, and α_2 represent the fractions of cationic, neutral, and anionic species, respectively.

Analysis of adsorption data

The adsorbed amount (i.e., q_e, mg/g) of SMT was calculated by the mass difference between the initial and final concentration as follows:

$$q_e = \frac{(C_i - C_e) \times V_w}{m_s} \quad (4)$$

where C_i and C_e are the initial and equilibrium SMT concentrations (mg/L), respectively; V_w (L) and m_s (g) represent the total SMT volume and the mass of the CM adsorbent, respectively.

Kinetic models

To investigate the reactive mechanism of SMT adsorption on each CM sample, kinetic adsorption data were analyzed by a pseudo-second-order model and an intra-particle diffusion (IPD) model. These models are introduced briefly below:

The pseudo-second-order model (Ho and McKay 1999) was developed based on the assumption that adsorption capacity is proportional to the number of active sites occupied on the CM samples, and the rate-limiting step involved in chemisorptions (Ho et al. 2000). The equation is expressed as follows:

$$\frac{dq_t}{dt} = k_{PSO}(q_e - q_t)^2 \quad (5)$$

By integrating Eq. (5) with the boundary conditions, $t = 0$ to $t = t$, and $q_t = 0$ to $q_t = q_t$, Eq. (6) is obtained:

$$q_t = \frac{k_{PSO} q_e^2 t}{1 + k_{PSO} q_e t} \quad (6)$$

where k_{PSO} (g/mg h) is the pseudo-second rate constant.

The IPD model was used to explain either the boundary layer diffusion or IPD during the adsorption processes (Cheung et al. 2007; Hassan and Yasin 2015). The equation can be expressed as follows (Singh et al. 2012):

$$q_e = kt^{1/2} + C \quad (7)$$

where kt is the IPD rate constant (mg/g $h^{1/2}$), and the C value is the intercept.

Freundlich isotherm

The Freundlich isotherm was used here to simulate the adsorption data of SMT on CM samples because it is suitable for heterogeneous systems and reversible adsorption (İlbay et al. 2015). The basic Freundlich equation is:

$$q_e = K_F \times C_e^{1/n} \quad (8)$$

The equation can be rearranged into a linear form as well (Kaniou et al. 2005):

$$\log q_e = \log K_F + \frac{1}{n} \log C_e \quad (9)$$

where q_e and C_e are the equilibrium concentrations of SMT in the adsorbed (mmol/kg) and aqueous phases (mmol/L), respectively. K_F (mmol/kg)/(mmol/L)$^{1/n}$ is the Freundlich adsorption capacity parameter. The slope ($1/n$) and the intercept ($\log K_F$) were obtained with the linear form of the Freundlich equation (Eq. 9). The n value is a heterogeneity constant, which defines the adsorption nonlinearity. For example, $n = 1$ (linear isotherm) indicates that the adsorption is homogeneous, and there is no interaction between the SMT species (Rauf et al. 2008).

Results and discussion

Characterizations of the carbonized CMs

The elemental compositions of the CM samples (Table 1) demonstrated that the hydrogen/carbon (H/C) atomic ratios decreased from 0.78 to 0.38 with increased carbonization

Table 1 Elemental and BET analyses of cow manure-based carbon (CMs) and CMs carbonized at 400, 600, and 800 °C

Adsorbent	CM400	CM600	CM800
Carbon (C, %)	66.4	67.4	68.7
Hydrogen (H, %)	4.3	3.2	2.2
Oxygen (O, %)	17.2	12.8	11.7
H/C[a]	0.78	0.57	0.38
O/C	0.19	0.14	0.13
Specific surface area (m^2/g)	2.97	142.10	114.66
Total pore volume (cm^3/g)	0.007	0.091	0.072
Average pore size (d, nm)	10.26	2.63	2.55
pH_{ZPC}^b	4.9	5.4	5.8

[a] Aromatic ratio

[b] Zero point charge of pH

temperatures. The CM samples with lower H/C ratios showed enrichment of the aromatic domains in their structures. The oxygen/carbon (O/C) atomic ratios of the CM samples, which represent the polarity, likely decreased from 0.19 to 0.13 when the temperature was increased. Thus, the CM samples would become more aromatic, with fewer polar functional groups, when they were carbonized at a higher temperature (Ahmad et al. 2012). The sums of the carbon, hydrogen, and oxygen content of each CM sample contributed to approximately 82.60–87.90 % (w/w) of the total weight. Other elements, such as N, P, and S, or residual ash or soil minerals, may be responsible for the remaining portion of the CM samples.

The SEM images of RCM and CM samples are shown in Fig. S3. We found that the surfaces of the RCM sample were rough and had a large, oval-shaped pore structure. When the carbonization temperature was increased to 400 °C, the surface of the RCM decomposed in part and developed a fine pore structure, as evidenced by the BET results (Table 1). The surface morphology became more smooth and irregular when the carbonization temperature increased to 600 °C (Fig. S3).

The BET results indicated that the SSA of the RCM and CM400 was relatively low, with values of 1.27 and 2.97 m^2/g, respectively (Table S1). A significant increase in SSA was observed when the carbonization temperature was increased to 600 (142.10 m^2/g) and 800 °C (114.66 m^2/g). The SSA of CM400 was lower than that of CM600, which was attributed to the inhibition of pore formation because of the greater presence of ash and volatile organic content on the surfaces of the CM400 (Subedi et al. 2016). Compared to those of CM600, slight decreases in SSA and total pore volume were observed for CM800, due likely to the collapse of the pore structures at 800 °C. These results are similar to those reported by Jeong et al. (2016), who found a slight decrease in SSA in sugarcane leaves/trash when the carbonization temperature was increased to 650 °C. The total pore volumes of RCM and CM samples increased from 0.007 to 0.090 cm^3/g with increased temperatures (Table S1). Because the CM600 and CM800 samples exhibited a greater SSA and total pore volumes, it may be helpful to adsorb more SMT in their structures.

The FTIR spectra of RCM and CM samples showed an intense, broadband ranging from 3100 to 3650 cm^{-1} that represented the hydrogen-bonded OH vibration (Fig. 1; Table S2) (Dutta et al. 2015). The peaks at 2937 and 2854 cm^{-1}, which were found in the RCM and CM400 samples, were attributed to –CH2 and –CH3 stretching in the aliphatic structures of cellulose and hemicelluloses (Wu et al. 2012). The peak at 1731 cm^{-1}, indicating –C=O stretching (Huck 2015), existed in all CM samples, but disappeared gradually at increased carbonization

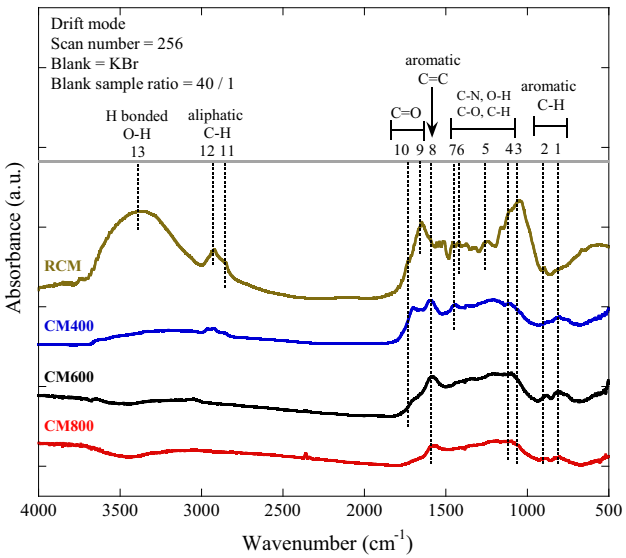

Fig. 1 FTIR spectra of raw cow manure (RCM) carbonized at 400, 600, and 800 °C, denoted as CM400, CM600, and CM800, respectively

temperatures (Table S2). The peak at 1652 cm^{-1} was found only for RCM and was attributed to carbonyl stretching of N–C=O in the peptide (Cantrell et al. 2012). The peak disappeared when the carbonization temperature was increased to 400 °C. The peak at 1590 cm^{-1} was attributed to C=C, C=O, and C=N stretching in the aromatic rings (Keiluweit et al. 2010). Multiple broad peaks were found in the region between 1000 and 1550 cm^{-1}, which were co-contributed by the C–O stretching in ethers, esters, and carbonates (1063 cm^{-1}) (Chia et al. 2012), C–O–C stretching in lignocelluloses (1110 cm^{-1}) (1110 cm^{-1}) (Keiluweit et al. 2010), the C–N stretching (1250 cm^{-1}) (Pena et al. 2001), OH deformation of carboxylate/carboxylic structures (1426 cm^{-1}) (Parker 1971), or C–H deformation of the phenolic lignin and aliphatic domains (1450 cm^{-1}) (Artz et al. 2008). The two peaks at 781 and 877 cm^{-1}, attributed to the aromatic –CH out-of plane vibration, indicated the presence of an adjacent aromatic hydrogen (Chen et al. 2015; Das et al. 2009). In summary, the FTIR spectra of CM samples indicated that the RCM and CM400 samples contained more O-containing functional groups and aliphatic structures (Fig. 1). However, with an increase in the carbonization temperature, these groups disappeared, while the peak intensities increased at 1590, 877, and 781 cm^{-1} and were designated as C=C/C=O stretching and C–H bending in the aromatic domains, respectively. When the carbonization temperature was increased to 800 °C, those functional groups on the CM surfaces disappeared, consistent with the results of elemental analyses that the CM structures became more aromatic and less polar at increased carbonization temperatures.

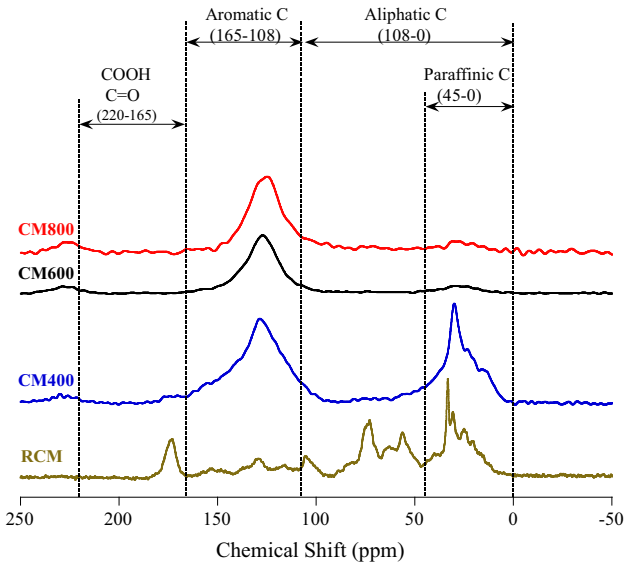

Fig. 2 Solid-state ^{13}C CP/MAS NMR spectra for raw cow manure (RCM), and CM400, CM600, and CM800 samples

The ^{13}C CP-MAS NMR spectra (Fig. 2) of the RCM and CM samples showed the temperature dependence of the aliphatic C region (0–108 ppm), aromatic C (108–165 ppm), and O-containing C (165–220 ppm) (Jung et al. 2013). While the RCM samples had the highest proportion of aliphatic and O-containing C, aromatic C was absent from the structure (Fig. 2). After the RCM samples were carbonized at 400 °C, the peak in the paraffinic C (0–45 ppm) region remained, but there was a substantial increase in the intensity of the aromatic C. When the carbonization temperature was increased to 600–800 °C, only aromatic C was found in the CMs. Thus, the CM800 contained relatively higher ratios of aromatic functional groups (Fig. 2). The NMR results were consistent with the elemental analysis and FTIR data, indicating again that the structures of CM600 and CM800 samples exhibited more aromaticity and less polarity.

Effects of pH on SMT adsorption in carbonized CM samples

The results of kinetic experiments indicated that the SMT adsorption in each CM sample reached a plateau after 12 h of reaction time (Fig. 3). At pH 3, the amount of SMT adsorbed on CM400, CM600, and CM800 was approximately 0.56, 3.55, and 3.79 mg/g, respectively, at 12 h (Fig. 3a). At pH 8, SMT adsorption on CM samples decreased significantly, and <1 mg/g SMT was adsorbed when the solution's pH was increased further to 10 (Fig. 3b, c). The CM600 and CM800 that bore higher SSAs and total pore volumes may have contributed in part to a greater adsorption of SMT in these samples. The maximum

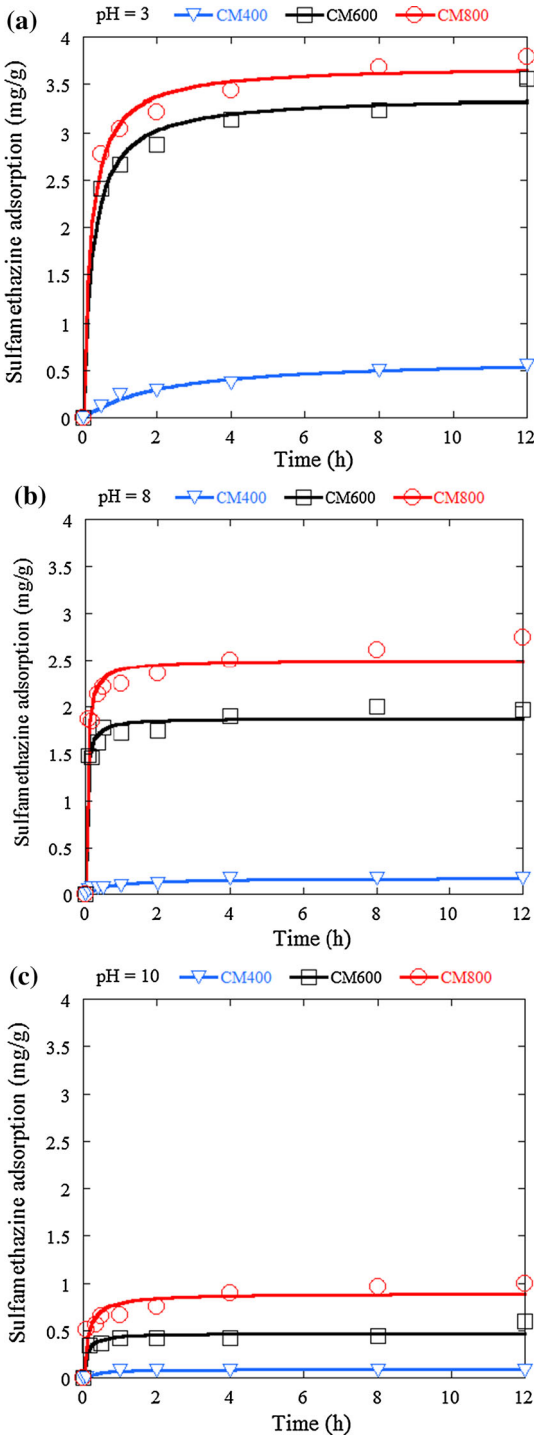

Fig. 3 Adsorption kinetics of sulfamethazine (SMT) on CM400, CM600, and CM800 at **a** pH 3, **b** pH 8, and **c** pH 10. The *lines* were obtained from the results of simulation using pseudo-second-order model

adsorption of SMT occurred at pH 3, and the CM800 exhibited a much greater ability to adsorb SMT at the pHs tested. The greatest efficiency in removal of CM800 may be ascribed to its relatively high aromatic content. According to the elemental analyses, the proportion of the

O/C ratio was the smallest in CM800 compared to that in CM600 and CM400 (Table 1), implying that the largest loss of oxygen content occurred after the 800 °C treatment of the CM. Such treatment would produce more basic and hydrophobic structures, and thus, more π electrons were distributed on the CM800 surfaces and were favorable for π–π interactions for SMT adsorption (Ahmad et al. 2012) (please see below).

Although the neutral (SMT^0) and positively charged SMT (SMT^+) coexisted in the solution at pH 3, SMT^0 was the dominant species (70 %). At pH 8, the proportion of SMT^0 decreased to approximately 20 % and negatively charged SMT (SMT^-) increased to 80 %. At pH 10, the SMT^- was the major species (near 100 %: Fig. S2). Because the pH_{zpc} of CM samples ranged from 4.90 to 5.80 (Table 1), an electrostatic repulsion occurred between SMT and CM at pH 3 (positive repulsion) and pH 8–10 (negative repulsion). Therefore, the electrostatic interactions might not play an important role in the determination of SMT adsorption on CMs. Xie et al. (2014) reported that the protonated SMT, i.e., SMT^+, and the neutral species of SMT were more effective π electron acceptors than was the anionic form of SMT due to the electron-withdrawing ability of the positively charged amino groups of SMT. Because the π electrons on the aromatic ring of SMT would be polarized and accompanied by a decrease in the electron density at low pH, electrostatic repulsion between the aromatic rings of SMT and the π electric properties in the benzene ring of SMT structure decreased concurrently (Xie et al. 2014). Thus, an enhancement of the π^+–π interactions between the polarized SMT molecules and electron-rich aromatic rings of the CM samples was expected at a higher carbonization temperature and under acidic conditions (Teixido et al. 2011). Therefore, SMT adsorption was favorable on the hydrophobic surfaces of CM800 at pH 3. At a pH of 8 and 10, both SMT and CM surfaces bore negative charges (Fig. S2). Due to the electrostatic repulsion, adsorption of anionic SMT on negatively charged CM surfaces was insignificant in alkaline conditions.

The adsorption kinetics of SMT on CM samples could be described well by a pseudo-second-order kinetic model, and all of the coefficient of determination (r^2) values were greater than 0.94 (Table 2). The maximum adsorption capacity was found on CM800 at pH 3, and the q_e values decreased with increasing pH, consistent with the adsorption results shown in Fig. 3. For each CM sample, the k_{pso} values increased as the pH increased from 3 to 10 (Table 2). These results might be attributed to the steric effects with increasing surface loadings. Although SMT was removed favorably by CMs at a lower pH, an increase in the surface loadings might limit the migration and reactivity of SMT toward the adsorptive sites of CMs. Thus, an increase in k_{pso} was observed when the solution's pH increased. Moreover, an increased pH would create a condition favorable for the dispersion of CM particles, and thus, SMT diffusion among the particles was achieved more readily. At pH 3, SMT adsorption on CM400 occurred very slowly, with a k_{pso} of 0.73 g/mg h, likely due to the presence of more O-containing functional groups associated with a lower SSA and total pore volume (Table 1; Fig. 1). In addition, the slow adsorption of SMT on CM400 might be ascribed to the electric repulsions between SMT^+ molecules and CM400 surfaces enriched with functional groups, such as amino or aromatic N-groups on the carbon black having the same electric properties (Fig. 1). In contrast, rapid adsorption of SMT on CM600 and CM800 might be attributed in part to a larger SSA and total pore volume in the structures of the CM samples (Table 2).

An IPD model was also used to describe the adsorptive behavior of SMT molecules on CMs (Fig. 4). An IPD graph was produced by plotting the q_e against $t_{1/2}$ (Fig. 4). The k_t and C values were calculated from the slope and intercept, respectively. Sulfamethazine adsorption on each CM could be described well by IPD model ($r^2 > 0.95$, Table 2). The number of intercepts in the plots suggested that adsorption was a multistep process (Liu et al. 2015). The plot in Fig. 4 shows two linear segments when SMT was adsorbed on CM600 and CM800 at a pH of 3 and 8, but such adsorptive behavior was not found on the CM400 sample (Fig. 4a, b). At a pH of 10, SMT adsorption on each CM adsorbent exhibited only one linear segment (Fig. 4c). The first sharper step shown in Fig. 4 was attributed to the rapid external surface adsorption correlated with the boundary layer diffusion of the SMT molecule (i.e., bulk phase to boundary layer). The external diffusion rate (kt_1) of SMT onto CMs decreased with increasing pH, and the CM400 showed the lowest diffusion rate in the first stage (external surfaces adsorption) at each pH (Table 2). These results indicated that the diffusion of SMT on CM400 surfaces was unfavorable, likely because the pH_{zpc} and SSA were lowest, and polarity was highest, thereby leading to greater electrostatic repulsion force between the O-containing functional groups of the CM400 surfaces and SMT. The second step was a gradual adsorption step, involving the diffusion of SMT into the pore structures of the CM samples, controlled by IPD (Zhou et al. 2014). Because the BET results indicated that CM600 and CM800 contained higher total pore volumes, but smaller pore sizes (Table 2), the slow, second step diffusion of SMT occurred only in these samples. The second step of the pore diffusion rate (kt_2) for SMT onto CM600 and CM800 also decreased when the solution's pH was increased from 3 to 8, indicating that the electrostatic forces induced by pH changes could influence SMT diffusion within the pores. At a pH of 3 and 8, SMT adsorption on CM600 and CM800 samples was controlled by both external adsorption and intra-

Table 2 Parameters of the pseudo-second-order model (PSO) and intra-particle diffusion model (IPD) for the adsorption kinetics of sulfamethazine on CM samples at pH 3, 8, and 10

Adsorbent	pH	Pseudo-second-order kinetic model			Intra-particle diffusion model					
					First stage[c]			Second stage[d]		
		q_e[a]	k_{PSO}[b]	r^2	kt_1[e]	C_1	r_1^2	kt_2[e]	C_2	r_2^2
CM400										
	3	0.63	0.73	0.99	0.16	0.04	0.99		NA[f]	
	8	0.17	9.30	0.96	0.03	0.06	0.89			
	10	0.09	32.75	0.97	0.009	0.052	0.99			
CM600										
	3	3.36	1.37	0.99	1.25	1.44	0.99	0.27	2.40	0.95
	8	1.88	16.37	0.99	0.47	1.30	0.81	0.11	1.65	0.95
	10	0.47	25.50	0.94	0.06	0.33	0.94		NA	
CM800										
	3	3.62	1.92	0.99	1.50	1.79	0.99	0.27	3.01	0.95
	8	2.52	8.42	0.98	0.57	1.72	0.90	0.17	2.11	0.99
	10	0.89	8.65	0.95	0.16	0.50	0.99		NA	

[a] Adsorption capacity with a unit of mg/g

[b] k_{pso} indicated pseudo-second-order kinetic adsorption rate constant with a unit of g/mg h

[c,d] Fitting process of IPD model (see Eq. 7)

[e] $kt_{1,2}$ indicated intra-particle diffusion rate constant with a unit of mg/g $h^{1/2}$

[f] NA = not available by IPD model

diffusion processes; however, only the external adsorption of SMT occurred on these two adsorbents at pH 10. This may indicate that SMT adsorption on CM samples proceeded rapidly, with the highest k_{pso} at pH 10 (Table 2). The absence of the second step of SMT adsorption on CM400 suggested the absence of efficient pore volumes or limited/inaccessible pores in CM400 due to the presence of a large amount of polar functional groups. Further, the development of positive charges on the polar groups of the CM400 surfaces may inhibit the boundary layer diffusion of hydrophobic molecules of SMT, and thus, the kinetic adsorption of SMT on CM400 was low at pH 3.

The C values in the IPD model indicated the thickness of the boundary layer, and the magnitudes of C represented the contributions of each stage to the rate-limiting step (Doğan et al. 2004). All of the positive C values in Table 2 suggested that adsorption of SMT on CMs occurred rapidly (Wu et al. 2009). We also found that the C_2 exhibited a higher value than that of C_1 for both the CM600 and CM800 samples, and the differences were the greatest at pH 3 (Table 2). These results indicated that the IPD (i.e., the second stage of SMT adsorption) might play a relatively important role in controlling SMT adsorption on CM600 and CM800 at a lower pH (Kannan and Sundaram 2001). We presumed that the IPD processes might lead to lower rate constants (k_{pso}) of SMT adsorption on CM600 and CM800 at pH 3, as given in Table 2.

Based on the results of the adsorption kinetics model, the functional groups on CM surfaces, SSA, total pore volume, and the SMT species largely controlled the kinetic adsorption processes. For instance, surface charges that developed on the polar and carboxylic groups on the surfaces of CM400 resulted in electrostatic repulsion between SMT and CM400, and thus, a relatively lower adsorption capacity was observed by comparison to that of CM600 and CM800 (Fig. 3; Table 2). These results were similar to those reported by Xie et al. (2014), who found that an increase in the mole fraction of deprotonated species of sulfamethoxazole (SMX) and sulfapyridine (SPY) led to an increase in electrostatic repulsion between the anionic forms of adsorbate molecules and the deprotonated O functionalities of biochars. Considering the aromatic rings of SMT and the hydrophobic properties of the CM surfaces, a hydrophobic partition interaction might also contribute to SMT adsorption on CMs. However, hydrophobic partitioning interactions dominated the SMT adsorption on CM samples only under neutral conditions, because such partitioning interactions could be overwhelmed by the electrostatic force (Lian et al. 2014). Therefore, hydrophobic partitioning interactions might contribute insignificantly to SMT adsorption on CM samples at high pH.

Sulfamethazine adsorption on CMs as influenced by ionic strengths

Based on the results above, CM800 showed the greatest adsorption capacity for SMT at each pH; therefore, this

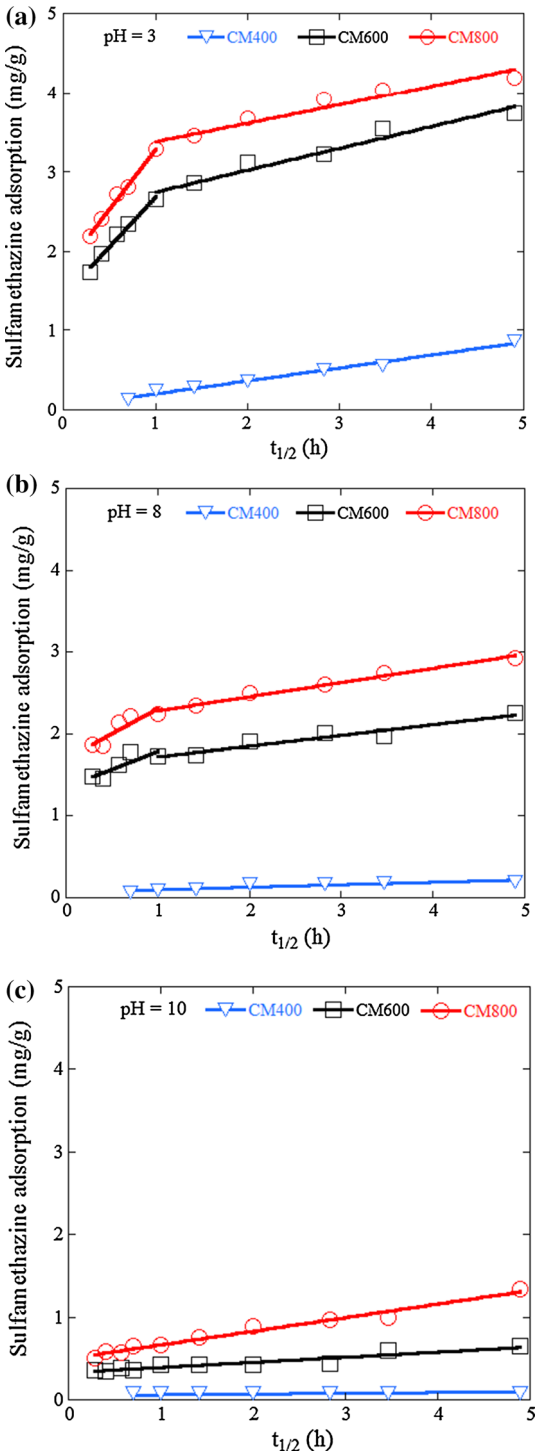

Fig. 4 Simulation results of intra-particle diffusion model for adsorption kinetics of sulfamethazine (SMT) on CM400, CM600, and CM800 at **a** pH 3, **b** pH 8, and **c** pH 10

sample was selected as a representative to investigate the effects of ionic strength on SMT adsorption (Fig. 5). The results showed that adsorption on CM800 was inhibited slightly at a higher ionic strength, and the adsorption was described well by the Freundlich model.

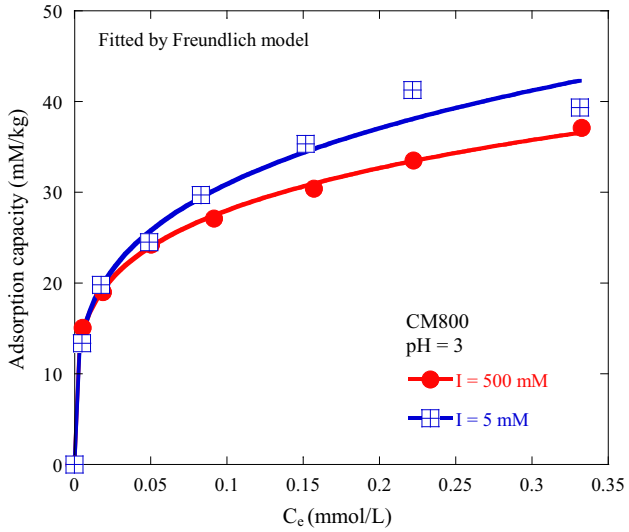

Fig. 5 Effects of ionic strengths on sulfamethazine (SMT) adsorption on CM800

At pH 3, the adsorption constant (K_F) for SMT on CM800 increased slightly from 46.80 to 56.50 (mmol/kg)/(mmol/L)$^{1/n}$ when the KCl concentrations decreased from 500 to 5 mM, indicating that the adsorption intensity increased with decreasing KCl concentrations. The removal of SMT on CM800 decreased by approximately 7 % when the KCl concentration increased from 5 to 500 mM (Table S3). Similar results were also found by Pavlovic et al. (2014), who proposed that an increase in ionic strength would result in a decrease in surface charges and thus would produce a decrease in the interaction of protonated SMT with the adsorbent surfaces. Qiang et al. (2013) also reported that the presence of 10 mM of chlorite-containing electrolytes could decrease SMT adsorption on magnetic mesoporous nanocomposite by 10–20 %. As mentioned previously, we proposed that the π^{+}–π EDA was the dominant force in SMT adsorption onto CM samples, and the effects of electrostatic interactions on SMT adsorption were insignificantly compared to those studies that have used adsorbents with more hydrophilic surfaces. Thus, a slight decrease in the capacity to adsorb SMT (ca. 7 %) on CM800 was observed at a higher ionic strength.

To evaluate the adsorption efficiency of the CM800 adsorbents for SMT obtained in this study, the adsorption capacity and Freundlich isotherm constants were compared to their counterparts reported in the literature, and the results are shown in Table S3 (Ben et al. 2014; Guo et al. 2013; Pavlovic et al. 2014; Qiang et al. 2013; Rajapaksha et al. 2014, 2015; Subedi et al. 2016). Compared with other adsorbents, the CM800 sample showed a relatively high adsorption capacity, in which the maximum adsorption capacity of 39.40 mM/kg SMT on CM800 was obtained at

pH 3 with 5 mM KCl. In addition, the adsorption intensity, indicated by K_F (Freundlich isotherm constants), was greater than that of other adsorbents (Table S3). Based on these results, the CM800 sample can serve as an efficient and low-cost adsorbent for SMT removal.

Conclusion

Carbonization of cow manure is an effective method to convert these waste materials to black carbon-like compounds with low polarity and high aromaticity. The temperature treatments also lead to a significant increase in SSA and total pore volume. The SSA and total pore volume of CM600/CM800 were approximately 114.66–142.10 m^2/g and 0.07–0.09 cm^3/g, respectively, much higher than were those of RCM/CM400 samples with SSA of 1.27–2.97 m^2/g and total pore volume of 0.003/0.007 cm^3/g. Therefore, the highest efficiency in the removal of SMT was obtained in CM600 (77.90 %) and CM800 (87.70 %) samples. The adsorption of SMT on CM samples could be described by a pseudo-second-order kinetic model and an IPD model.

At pH 3, SMT antibiotic was adsorbed strongly on CM800 through the π^+–π interaction, and as much as 3.62 mg/g of SMT was adsorbed. However, when the pH was raised to 10, the increase in the proportion of the anionic form of SMT decreased the π^+–π interaction between SMT and CMs, leading to a significant decrease in SMT adsorption (0.89 mg/g). Electrostatic repulsion between anionic SMT and negatively charged CM surfaces was responsible for the decrease in adsorption capacity of SMT under alkaline conditions. The results of ionic strength experiments showed a slight effect on the adsorption efficiency of SMT on CMs, likely due to the absence of electrostatic interactions between SMT and the CM sample. Our results demonstrated that CM samples derived from carbonization of cow manure can be used as an efficient adsorbent to remove SMT at low to neutral pH levels and may serve as a low-cost substitute for the activated carbon in scavenging pharmaceutical products.

Acknowledgments The work was financially supported by the Ministry of Science and Technology, ROC under Project Nos. 101-2621-M-005-005, 102-2621-M-005-001, and 103-2621-M-005-002, and, in part, by the Ministry of Education, ROC under the Aim for Top University (ATU) plan.

References

Ahmad M, Lee SS, Dou XM, Mohan D, Sung JK, Yang JE, Ok YS (2012) Effects of pyrolysis temperature on soybean stover- and peanut shell-derived biochar properties and TCE adsorption in water. Bioresour Technol 118:536–544. doi:10.1016/j.biortech.2012.05.042

Artz RRE, Chapman SJ, Jean Robertson AH, Potts JM, Laggoun-Défarge F, Gogo S et al (2008) FTIR spectroscopy can be used as a screening tool for organic matter quality in regenerating cutover peatlands. Soil Biol Biochem 40:515–527. doi:10.1016/j.soilbio.2007.09.019

Bao X, Qiang Z, Chang J-H, Ben W, Qu J (2014) Synthesis of carbon-coated magnetic nanocomposite (Fe_3O_4@C) and its application for sulfonamide antibiotics removal from water. J Environ Sci 26:962–969. doi:10.1016/S1001-0742(13)60485-4

Barbooti MM, Su H, Punamiya P, Sarkar D (2014) Oxytetracycline sorption onto Iraqi montmorillonite. Int J Environ Sci Technol 11:69–76. doi:10.1007/s13762-013-0361-6

Batt AL, Snow DD, Aga DS (2006) Occurrence of sulfonamide antimicrobials in private water wells in Washington County, Idaho, USA. Chemosphere 64:1963–1971

Ben WW, Qiang ZM, Yin XW, Qu JH, Pan X (2014) Adsorption behavior of sulfamethazine in an activated sludge process treating swine wastewater. J Environ Sci China 26:1623–1629. doi:10.1016/j.jes.2014.06.002

Braschi I, Blasioli S, Gigli L, Gessa CE, Alberti A, Martucci A (2010) Removal of sulfonamide antibiotics from water: evidence of adsorption into an organophilic zeolite Y by its structural modifications. J Hazard Mater 178:218–225. doi:10.1016/j.jhazmat.2010.01.066

Bui TX, Pham VH, Le ST, Choi H (2013) Adsorption of pharmaceuticals onto trimethylsilylated mesoporous SBA-15. J Hazard Mater 254–255:345–353. doi:10.1016/j.jhazmat.2013.04.003

Cantrell KB, Hunt PG, Uchimiya M, Novak JM, Ro KS (2012) Impact of pyrolysis temperature and manure source on physicochemical characteristics of biochar. Bioresour Technol 107:419–428. doi:10.1016/j.biortech.2011.11.084

Chen C, Zhou W, Lin D (2015) Sorption characteristics of *N*-nitrosodimethylamine onto biochar from aqueous solution. Bioresour Technol 179:359–366

Cheung WH, Szeto YS, McKay G (2007) Intraparticle diffusion processes during acid dye adsorption onto chitosan. Bioresour Technol 98:2897–2904. doi:10.1016/j.biortech.2006.09.045

Chia CH, Gong B, Joseph SD, Marjo CE, Munroe P, Rich AM (2012) Imaging of mineral-enriched biochar by FTIR, Raman and SEM–EDX. Vib Spectrosc 62:248–257. doi:10.1016/j.vibspec.2012.06.006

Christian T, Schneider RJ, Farber HA, Skutlarek D, Meyer MT, Goldbach HE (2003) Determination of antibiotic residues in manure, soil, and surface waters. Acta Hydroch Hydrob 31:36–44. doi:10.1002/aheh.200390014

Das DD, Schnitzer MI, Monreal CM, Mayer P (2009) Chemical composition of acid-base fractions separated from biooil derived by fast pyrolysis of chicken manure. Bioresour Technol 100:6524–6532. doi:10.1016/j.biortech.2009.06.104

Doğan M, Alkan M, Türkyilmaz A, Özdemir Y (2004) Kinetics and mechanism of removal of methylene blue by adsorption onto perlite. J Hazard Mater 109:141–148. doi:10.1016/j.jhazmat.2004.03.003

Dutta B, Raghavan VGS, Orsat V, Ngadi M (2015) Surface characterisation and classification of microwave pyrolysed maple wood biochar. Biosyst Eng 131:49–64. doi:10.1016/j.biosystemseng.2015.01.002

Gao Y-q, Gao N-y, Deng Y, Gu J-s, Gu Y-l, Zhang D (2013) Factors affecting sonolytic degradation of sulfamethazine in water. Ultrason Sonochem 20:1401–1407. doi:10.1016/j.ultsonch.2013.04.007

García-Galán MJ, Díaz-Cruz S, Barceló D (2013) Multiresidue trace analysis of sulfonamide antibiotics and their metabolites in soils and sewage sludge by pressurized liquid extraction followed by liquid chromatography–electrospray-quadrupole linear ion trap mass spectrometry. J Chromatogr A 1275:32–40. doi:10.1016/j.chroma.2012.12.004

Guo XT, Yang C, Dang Z, Zhang Q, Li YJ, Meng QY (2013) Sorption thermodynamics and kinetics properties of tylosin and sulfamethazine on goethite. Chem Eng J 223:59–67. doi:10.1016/j.cej.2013.02.115

Hassan S, Yasin T (2015) Role of tailored surface of activated carbon for adsorption of ionic liquids for environmental remediation. Int J Environ Sci Technol 12:2711–2722. doi:10.1007/s13762-014-0678-9

Heberer T (2002) Occurrence, fate, and removal of pharmaceutical residues in the aquatic environment: a review of recent research data. Toxicol Lett 131:5–17

Hiba A, Carine A, Haifa AR, Ryszard L, Farouk J (2016) Monitoring of twenty-two sulfonamides in edible tissues: investigation of new metabolites and their potential toxicity. Food Chem 192:212–227. doi:10.1016/j.foodchem.2015.06.093

Ho YS, McKay G (1999) Pseudo-second order model for sorption processes. Process Biochem 34:451–465. doi:10.1016/S0032-9592(98)00112-5

Ho YS, Ng JCY, McKay G (2000) Kinetics of pollutant sorption by biosorbents: review. Sep Purif Methods 29:189–232. doi:10.1081/spm-100100009

Hou J, Yan J, Zhang F, Zhao Q, Chen H, Zhang Y et al (2014) Evaluation of intercalated α-zirconium phosphate as sorbent in separation and detection of sulfonamides in honey. Food Chem 150:58–64. doi:10.1016/j.foodchem.2013.10.144

Hu LH, Flanders PM, Miller PL, Strathmann TJ (2007) Oxidation of sulfamethoxazole and related antimicrobial agents by TiO_2 photocatalysis. Water Res 41:2612–2626. doi:10.1016/j.watres.2007.02.026

Huck CW (2015) Advances of infrared spectroscopy in natural product research. Phytochem Lett 11:384–393. doi:10.1016/j.phytol.2014.10.026

İlbay Z, Şahin S, Kerkez Ö, Bayazit ŞS (2015) Isolation of naproxen from wastewater using carbon-based magnetic adsorbents. Int J Environ Sci Technol 12:3541–3550. doi:10.1007/s13762-015-0775-4

Jeong CY, Dodla SK, Wang JJ (2016) Fundamental and molecular composition characteristics of biochars produced from sugarcane and rice crop residues and by-products. Chemosphere 142:4–13. doi:10.1016/j.chemosphere.2015.05.084

Ji LL, Chen W, Zheng SR, Xu ZY, Zhu DQ (2009) Adsorption of sulfonamide antibiotics to multiwalled carbon nanotubes. Langmuir 25:11608–11613. doi:10.1021/la9015838

Ji LL, Wan YQ, Zheng SR, Zhu DQ (2011) Adsorption of tetracycline and sulfamethoxazole on crop residue-derived ashes: implication for the relative importance of black carbon to soil sorption. Environ Sci Technol 45:5580–5586. doi:10.1021/es200483b

Jung C, Park J, Lim KH, Park S, Heo J, Her N et al (2013) Adsorption of selected endocrine disrupting compounds and pharmaceuticals on activated biochars. J Hazard Mater 263(Part 2):702–710. doi:10.1016/j.jhazmat.2013.10.033

Kaniou S, Pitarakis K, Barlagianni I, Poulios I (2005) Photocatalytic oxidation of sulfamethazine. Chemosphere 60:372–380. doi:10.1016/j.chemosphere.2004.11.069

Kannan N, Sundaram MM (2001) Kinetics and mechanism of removal of methylene blue by adsorption on various carbons—a comparative study. Dyes Pigments 51:25–40. doi:10.1016/S0143-7208(01)00056-0

Keiluweit M, Nico PS, Johnson MG, Kleber M (2010) Dynamic molecular structure of plant biomass-derived black carbon (Biochar). Environ Sci Technol 44:1247–1253. doi:10.1021/es9031419

Kim KR, Owens G, Ok YS, Park WK, Lee DB, Kwon SI (2012) Decline in extractable antibiotics in manure-based composts during composting. Waste Manag (Oxford) 32:110–116. doi:10.1016/j.wasman.2011.07.026

Kümmerer K (2009) The presence of pharmaceuticals in the environment due to human use—present knowledge and future challenges. J Environ Manag 90:2354–2366. doi:10.1016/j.jenvman.2009.01.023

Kurwadkar ST, Adams CD, Meyer MT, Kolpin DW (2007) Effects of sorbate speciation on sorption of selected sulfonamides in three loamy soils. J Agric Food Chem 55:1370–1376. doi:10.1021/jf060612o

Leal RMP, Alleoni LRF, Tornisielo VL, Regitano JB (2013) Sorption of fluoroquinolones and sulfonamides in 13 Brazilian soils. Chemosphere 92:979–985. doi:10.1016/j.chemosphere.2013.03.018

Li X, Yu H, Xu S, Hua R (2013) Uptake of three sulfonamides from contaminated soil by pakchoi cabbage. Ecotoxicol Environ Saf 92:297–302. doi:10.1016/j.ecoenv.2013.03.010

Lian F, Sun B, Song Z, Zhu L, Qi X, Xing B (2014) Physicochemical properties of herb-residue biochar and its sorption to ionizable antibiotic sulfamethoxazole. Chem Eng J 248:128–134

Lillenberg M, Yurchenko S, Kipper K, Herodes K, Pihl V, Lõhmus R et al (2010) Presence of fluoroquinolones and sulfonamides in urban sewage sludge and their degradation as a result of composting. Int J Environ Sci Technol 7:307–312. doi:10.1007/BF03326140

Lim SL, Lee LH, Wu TY (2015a) Sustainability of using composting and vermicomposting technologies for organic solid waste biotransformation: recent overview, greenhouse gases emissions and economic analysis. J Clean Prod. doi:10.1016/j.jclepro.2015.08.083

Lim SL, Wu TY, Lim PN, Shak KPY (2015b) The use of vermicompost in organic farming: overview, effects on soil and economics. J Sci Food Agric 95:1143–1156. doi:10.1002/jsfa.6849

Lin T, Chen Y, Chen W (2013) Impact of toxicological properties of sulfonamides on the growth of zebrafish embryos in the water. Environ Toxicol Pharmacol 36:1068–1076. doi:10.1016/j.etap.2013.09.009

Liu P, Liu WJ, Jiang H, Chen JJ, Li WW, Yu HQ (2012) Modification of bio-char derived from fast pyrolysis of biomass and its application in removal of tetracycline from aqueous solution. Bioresour Technol 121:235–240. doi:10.1016/j.biortech.2012.06.085

Liu N, Charrua AB, Weng C-H, Yuan X, Ding F (2015) Characterization of biochars derived from agriculture wastes and their adsorptive removal of atrazine from aqueous solution: a comparative study. Bioresour Technol 198:55–62. doi:10.1016/j.biortech.2015.08.129

Lopez-Ramon MV, Stoeckli F, Moreno-Castilla C, Carrasco-Marin F (1999) On the characterization of acidic and basic surface sites on carbons by various techniques. Carbon 37:1215–1221. doi:10.1016/s0008-6223(98)00317-0

Mansour D, Fourcade F, Soutrel I, Hauchard D, Bellakhal N, Amrane A (2015) Relevance of a combined process coupling electro-Fenton and biological treatment for the remediation of sulfamethazine solutions—application to an industrial pharmaceutical effluent. C R Chim 18:39–44. doi:10.1016/j.crci.2014.05.005

Parker FS (1971) Applications of infrared spectroscopy in biochemistry, biology and medicine. doi:10.1007/978-1-4684-1872-9

Pavlovic DM, Curkovic L, Blazek D, Zupan J (2014) The sorption of sulfamethazine on soil samples: isotherms and error analysis. Sci Total Environ 497:543–552. doi:10.1016/j.scitotenv.2014.08.018

Pena JM, Allen NS, Edge M, Liauw CM, Valange B (2001) Factors affecting the adsorption of fatty acids, alcohols and aromatic compounds on to carbon black pigments (flow micro-calorimetry studies). Dyes Pigments 49:29–49. doi:10.1016/s0143-7208(01)00004-3

Perez-Moya M, Graells M, Castells G, Amigo J, Ortega E, Buhigas G et al (2010) Characterization of the degradation performance of the sulfamethazine antibiotic by photo-Fenton process. Water Res 44:2533–2540. doi:10.1016/j.watres.2010.01.032

Pinna MV, Castaldi P, Deiana P, Pusino A, Garau G (2012) Sorption behavior of sulfamethazine on unamended and manure-amended soils and short-term impact on soil microbial community. Ecotox Environ Saf 84:242

Putra EK, Pranowo R, Sunarso J, Indraswati N, Ismadji S (2009) Performance of activated carbon and bentonite for adsorption of amoxicillin from wastewater: mechanisms, isotherms and kinetics. Water Res 43:2419–2430. doi:10.1016/j.watres.2009.02.039

Qiang ZM, Bao XL, Ben WW (2013) MCM-48 modified magnetic mesoporous nanocomposite as an attractive adsorbent for the removal of sulfamethazine from water. Water Res 47:4107–4114. doi:10.1016/j.watres.2012.10.039

Raich-Montiu J, Folch J, Compañó R, Granados M, Prat MD (2007) Analysis of trace levels of sulfonamides in surface water and soil samples by liquid chromatography-fluorescence. J Chromatogr A 1172:186–193. doi:10.1016/j.chroma.2007.10.010

Rajapaksha AU, Vithanage M, Zhang M, Ahmad M, Mohan D, Chang SX, Ok YS (2014) Pyrolysis condition affected sulfamethazine sorption by tea waste biochars. Bioresour Technol 166:303–308. doi:10.1016/j.biortech.2014.05.029

Rajapaksha AU, Vithanage M, Ahmad M, Seo DC, Cho JS, Lee SE et al (2015) Enhanced sulfamethazine removal by steam-activated invasive plant-derived biochar. J Hazard Mater 290:43–50. doi:10.1016/j.jhazmat.2015.02.046

Rauf MA, Bukallah SB, Hamour FA, Nasir AS (2008) Adsorption of dyes from aqueous solutions onto sand and their kinetic behavior. Chem Eng J 137:238–243. doi:10.1016/j.cej.2007.04.025

Richter D, Dünnbier U, Massmann G, Pekdeger A (2007) Quantitative determination of three sulfonamides in environmental water samples using liquid chromatography coupled to electrospray tandem mass spectrometry. J Chromatogr A 1157:115–121. doi:10.1016/j.chroma.2007.04.042

Schwab BW, Hayes EP, Fiori JM, Mastrocco FJ, Roden NM, Cragin D et al (2005) Human pharmaceuticals in US surface waters: a human health risk assessment. Regul Toxicol Pharm 42:296–312. doi:10.1016/j.yrtph.2005.05.005

Shirzad-Siboni M, Khataee A, Hassani A, Karaca S (2015) Preparation, characterization and application of a CTAB-modified nanoclay for the adsorption of an herbicide from aqueous solutions: kinetic and equilibrium studies. C R Chim 18:204–214

Singh SK, Townsend TG, Mazyck D, Boyer TH (2012) Equilibrium and intra-particle diffusion of stabilized landfill leachate onto micro- and meso-porous activated carbon. Water Res 46:491–499. doi:10.1016/j.watres.2011.11.007

Srinivasan P, Sarmah AK, Manley-Harris M (2014) Sorption of selected veterinary antibiotics onto dairy farming soils of contrasting nature. Sci Total Environ 472:695–703. doi:10.1016/j.scitotenv.2013.11.104

Subedi R, Taupe N, Pelissetti S, Petruzzelli L, Bertora C, Leahy JJ, Grignani C (2016) Greenhouse gas emissions and soil properties following amendment with manure-derived biochars: influence of pyrolysis temperature and feedstock type. J Environ Manag 166:73–83. doi:10.1016/j.jenvman.2015.10.007

Tamtam F, Mercier F, Le Bot B, Eurin J, Tuc Dinh Q, Clément M, Chevreuil M (2008) Occurrence and fate of antibiotics in the Seine River in various hydrological conditions. Sci Total Environ 393:84–95. doi:10.1016/j.scitotenv.2007.12.009

Teixido M, Pignatello JJ, Beltran JL, Granados M, Peccia J (2011) Speciation of the ionizable antibiotic sulfamethazine on black carbon (Biochar). Environ Sci Technol 45:10020–10027. doi:10.1021/es202487h

Tolls J (2001) Sorption of veterinary pharmaceuticals in soils: a review. Environ Sci Technol 35:3397–3406. doi:10.1021/es0003021

Valderrama C, Cortina JL, Farran A, Gamisans X, Lao C (2007) Kinetics of sorption of polyaromatic hydrocarbons onto granular activated carbon and Macronet hyper-cross-linked polymers (MN200). J Colloid Interface Sci 310:35–46. doi:10.1016/j.jcis.2007.01.039

Vieira EFS, Cestari AR, Oliveira CDS, de Lima PS, Almeida LE (2007) Thermodynamics of pyrimethamine and sulfadiazine binding to a chitosan derivative. Thermochim Acta 459:9–11. doi:10.1016/j.tca.2007.03.014

Wang X, Xing B (2007) Sorption of organic contaminants by biopolymer-derived chars. Environ Sci Technol 41:8342–8348

Wang C, Li H, Liao SH, Zhang D, Wu M, Pan B, Xing BS (2014) Sorption affinities of sulfamethoxazole and carbamazepine to two sorbents under co-sorption systems. Environ Pollut 194:203–209. doi:10.1016/j.envpol.2014.07.033

Wu F-C, Tseng R-L, Juang R-S (2009) Initial behavior of intraparticle diffusion model used in the description of adsorption kinetics. Chem Eng J 153:1–8. doi:10.1016/j.cej.2009.04.042

Wu W, Yang M, Feng Q, McGrouther K, Wang H, Lu H, Chen Y (2012) Chemical characterization of rice straw-derived biochar for soil amendment. Biomass Bioenergy 47:268–276. doi:10.1016/j.biombioe.2012.09.034

Xie MX, Chen W, Xu ZY, Zheng SR, Zhu DQ (2014) Adsorption of sulfonamides to demineralized pine wood biochars prepared under different thermochemical conditions. Environ Pollut 186:187–194. doi:10.1016/j.envpol.2013.11.022

Zessel K, Mohring S, Hamscher G, Kietzmann M, Stahl J (2014) Biocompatibility and antibacterial activity of photolytic products of sulfonamides. Chemosphere 100:167–174. doi:10.1016/j.chemosphere.2013.11.038

Zhou CJ, Wu QL, Lei TZ, Negulescu JI (2014) Adsorption kinetic and equilibrium studies for methylene blue dye by partially hydrolyzed polyacrylamide/cellulose nanocrystal nanocomposite hydrogels. Chem Eng J 251:17–24. doi:10.1016/j.cej.2014.04.034